

Effect of $\gamma\text{-Al}_2\text{O}_3$ /water nanofluid on the thermal performance of shell and coil heat exchanger with different coil torsions

K. M. Elshazly¹ · R. Y. Sakr¹ · R. K. Ali¹ · M. R. Salem¹

Received: 17 August 2016 / Accepted: 24 November 2016 / Published online: 30 November 2016
© Springer-Verlag Berlin Heidelberg 2016

Abstract This work investigated experimentally the thermal performance of shell and coil heat exchanger with different coil torsions (λ) for $\gamma\text{-Al}_2\text{O}_3$ /water nanofluid flow. Five helically coiled tube (HCT) with $0.0442 \leq \lambda \leq 0.1348$ were tested within turbulent flow regime. The average size of $\gamma\text{-Al}_2\text{O}_3$ particles is 40 nm and volume concentration (φ) is varied from 0 to 2%. Results showed that reducing coil torsion enhances the heat transfer rate and increases HCT-friction factor (f_c). Also, it is noticed that HCT average Nusselt number (Nu_t) and f_c of nanofluids increase with increasing $\gamma\text{-Al}_2\text{O}_3$ volume concentration. The thermal performance index, $TPI = (h_{t,nf}/h_{t,bf})/(\Delta P_{c,nf}/\Delta P_{c,bf})$, increases with increasing nanoparticles concentration, coil torsion, HCT-side inlet temperature and nanofluid flow rate. Over the studied range of HCT-Reynolds number, the average value of TPI is of 1.34 and 2.24 at $\varphi = 0.5\%$ and $\varphi = 2\%$, respectively. The average value of TPI is of 1.64 at $\lambda = 0.0442$ while its average value at $\lambda = 0.1348$ is of 2.01. One of the main contributions is to provide heat equipments designers with Nu_t and f_c correlations for practical configurations shell and coil heat exchangers with a wide range of nanofluid concentration.

List of symbols

Symbols

A Area, m^2
Cp Specific heat, $\text{J/kg } ^\circ\text{C}$

D Coil diameter, m
d Tube diameter, m
 f Fanning friction factor
h Average convection heat transfer coefficient, $\text{W/m}^2 \text{ } ^\circ\text{C}$
k Thermal conductivity, $\text{W/m } ^\circ\text{C}$
L Length, m
 \dot{m} Mass flow rate, kg/s
N Number of the turns of the helically coiled tube
De Dean number, $Re_t \delta_{0,5}$
Nu Average Nusselt number
P Pressure, Pa
Pr Prandtl number
p Pitch of helically coiled tube, m
Q Heat transfer rate, W
S Spacing of helically coiled tube, m
T Temperature, K
Re Reynolds number
U Overall heat transfer coefficient, $\text{W/m}^2 \text{ } ^\circ\text{C}$
u Axial velocity, m/s
 \dot{V} Volume flow rate, m^3/s

Scripts

Ave Average
b Bulk
bf Base fluid
c Coil
f Film
h Hydraulic
i Inner or inlet or internal
LM Logarithmic mean
nf Nanofluid
np Nanoparticle
s Surface
sh Shell

✉ R. K. Ali
Ragabkhalil1971@gmail.com;
Ragab.aboyazid@feng.bu.edu.eg

¹ Mechanical Engineering Department, Faculty of Engineering Shoubra, Benha University, 108 Shoubra Street, Cairo 11689, Egypt

m	Mean
t, o	Refers to the outer area of the surface of the HCT
t	Tube
o	Out or outer or overall

Greek letters

Δ	Differential
β	Ratio of the nano-layer thickness to the original particle radius
γ	Gamma
Γ	Modeling function was introduced in Eq. (2)
δ	Dimensionless coil curvature ratio
λ	Coil torsion
μ	Dynamic viscosity, kg/ms
ξ	Modeling function was introduced in Eq. (3)
ρ	Density, kg/m ³
φ	Particles volume concentration

Acronyms and abbreviations

Al ₂ O ₃	Alumina (aluminum oxide)
CuO	Copper oxide
HCT	Helically coiled tube
PVC	Polyvinyl chloride
EG	Ethylene glycol
TiO ₂	Titanium oxide
SiO ₂	Silicon oxide
TPI	Thermal performance index

1 Introduction

Helically coiled tubes have many industrial applications due to the compactness and promoting good fluid mixing that increase the heat transfer rate [1–12]. Lower thermal conductivity of working fluids stands behind lower heat transfer rate in industrial processes [13, 14]. Adding very high thermal conductivities of solid particles to conventional fluids is one way to overcome this problem [15].

Zamzamian et al. [16] experimentally studied the effect of forced convective heat transfer coefficient of Al₂O₃/EG and CuO/EG nanofluids in turbulent flow using a double pipe and plate heat exchangers. The findings indicate considerable enhancement in convective heat transfer coefficient of the nanofluids as compared to the base fluid. Moreover, the results indicated that with increasing φ and nanofluid temperature, the heat transfer coefficient of nanofluid increases. Peyghambarzadeh et al. [17] experimentally compared the heat transfer performance of pure water and pure EG with their binary mixtures in laminar region in flattened tubes of car radiator. Furthermore, the heat transfer performance of the car radiator was determined for different φ (0.1–1%) of Al₂O₃ (20 nm). The results demonstrated that nanofluids clearly enhance heat transfer compared to

their own base fluid; 40% enhancement in the heat transfer coefficient was recorded. Also, the heat transfer behaviors of the nanofluids are highly depended on φ and Re, and weakly dependent on the temperature. Peyghambarzadeh and Jamnani [18] repeated same experiments in turbulent region, in which same trends were recorded. Razi et al. [19] experimentally studied the heat transfer and pressure drop characteristics of CuO (50 nm, 0.2–2 wt.)/oil nanofluid flow inside horizontal flattened isoflux tubes in laminar region. Observations showed that the heat transfer performance is improved as the tube profile was flattened. Furthermore, using nanofluid instead of base fluid and flattening the tube profile results in pressure drop increasing. Furthermore, applying flattened tubes instead of round tube is more effective to enhance the convective heat transfer coefficient compared to using nanofluids instead of the base liquid. Moraveji et al. [20] numerically investigated the convective heat transfer coefficient in the developed region of horizontal tube flow containing non-Newtonian nanofluid; Al₂O₃ (45 and 150 nm, 1–6 wt.)/Xanthan aqueous solutions, with constant heat flux. Results showed that the heat transfer coefficient is enhanced with increasing φ and Re, while decreases with increasing particle diameter. Hussein et al. [21] experimentally and numerically studied the friction factor and forced convection heat transfer of SiO₂ (1–2.5 vol.)/water nanofluid conducted in a car radiator. Results showed that Nu_{nf} and friction factor increase with increasing φ at the same flow rate. The authors noticed that applying SiO₂ nanofluid enhances Nu_{nf} with average increase of 50% as a comparison with pure water. Kumar et al. [22] presented an experimental investigation on a shell and coil heat exchanger using nonmetallic sisal nanofluid ($\varphi = 0.5\%$) constant coil torsion and curvature. They reported that the overall heat transfer coefficient increased with increasing φ . Humnic and Humnic [23] introduced a numerical study on the thermal performance of using CuO and TiO₂ nano-powders to enhance water thermal conductivity applied in double tube helical heat exchanger. The nano-powder diameter was of 24 nm with concentration range of 0.5–3%. They showed that applying CuO/water and TiO₂/water significantly augments heat transfer coefficient and the enhancement increases with Dean number and nano-powder concentration. Hashemi and Akhavan-Behabadi [24] investigated the thermal performance characteristics of flowing CuO/oil with powder diameter of 50 nm and 0.5–2 wt.% concentration in HCT with constant heat flux. The maximum enhancement in convective heat transfer coefficient is of 18.7 and 30.4% for straight tube and HCT at $10 \leq Re \leq 100$, respectively. Kumar et al. [25–28] experimentally studied heat transfer and pressure drop of γ -Al₂O₃ (0.1, 0.4 and 0.8 vol.)/water nanofluid in HCT of shell and coil heat exchanger. The experiments were carried out using one heat exchanger geometry in

horizontal and vertical positions, in addition to counter and parallel flow configurations for $1600 < De < 2700$ and $5200 < Re_t < 8600$. The findings indicated that there is no considerable effect on Nu_t by changing flow configuration. It was shown also a considerable increase in the convective heat transfer coefficient and pressure drop with increasing φ . An average increase in Nu_t and f_c is of 45 and 21% compared with pure water, respectively, in horizontal position. While the average increase in vertical position was of 49 and 25%, respectively.

Salem et al. [29–31] carried out a test rig to investigate the thermal performance of shell and coil heat exchanger. The test section has the facility to change the helical coil to investigate the effect of coil curvature and torsion. Salem et al. [29] constructed five heat exchangers of counter flow configuration such that HCT torsion, λ , increases from 0.0442 to 0.1348 with the same curvature of 0.0591. They performed all experiments on pure water within $6511 \leq Re_t \leq 62,091$. The results show that the average increase in HCT Nusselt number is of 108.7 and 58.6%, respectively, when λ decreases from 0.1348 to 0.0442. Also, the average increase in shell Nusselt number is of 173.9 and 69.5%, respectively, when λ decreases from 0.1348 to 0.0442. Other five heat exchangers were constructed with same coil torsion ($\lambda = 0.0895$) to test the effect of coil curvature ($0.0392 \leq \delta \leq 0.1194$) for water and $\gamma\text{-Al}_2\text{O}_3/\text{Water}$ Nanofluid [30, 31]. The results of water in both sides presented in Ref. [30] showed that the average increase in the average Nusselt number is of 160.3–80.6% for the HCT side and of 224.3–92.6% for the shell side when δ increases from 0.0392 to 0.1194. In addition, the associated increase in HCT-Fanning friction factor is of 33.2–7.7% within $0.0392 \leq \delta \leq 0.1194$. Salem et al. [31] performed the tests for $\gamma\text{-Al}_2\text{O}_3/\text{water}$ nanofluid with average size of 40 nm and particles volume concentration (φ) from 0 to 2% for $0.0392 \leq \delta \leq 0.1194$. Correlations for the average Nusselt numbers for both heat exchanger sides and the HCT Fanning friction factor as a function of HCT-Reynolds number, Prandtl number and particles volume concentration within $0.0392 \leq \delta \leq 0.1194$, $0.5 < \varphi \leq 2\%$ and $1.92 \leq Pr_t \leq 3.9$. The present work aims to study the effect of coil torsion on characteristics of convective heat transfer for $\gamma\text{-Al}_2\text{O}_3/\text{water}$ nanofluid flow with average size of 40 nm and particles volume concentration (φ) from 0.5 to 2%. The present measurements were utilized to provide experimental Nusselt number and friction factor correlations that help in design of heat transfer equipments.

2 Experimental setup

The experimental runs were conducted on the test rig that built in 2014 and proposed for testing different heat transfer

equipments. The test rig is composed of heating and cooling closed loops as shown in Fig. 1. The hot loop consists of heating unit, pump, valves, HCT, flow meter and the connecting pipes. The cold circuit consists of cooling unit, pump, valves, shell, flow meter and the connecting pipes. The rating power of the electric heater used in the heating loop is of 6 kW. Two cooling units of 10.5 kW were used to achieve heat removal in the cooling circuit. Five helical coils were constructed such that coil torsion ($\lambda = p_c/\pi D_c$) is varied from 0.0442 to 0.1384 with constant curvature ($\delta = d_{t,i}/D_c$) of 0.0591. The HCTs were formed from straight copper tubes of the same length 4415, 9.52 mm outer diameter and 8.3 mm inner diameter. Schematic diagram of the shell and coil heat exchanger is shown in Fig. 2 and the characteristic dimensions of the different configurations are revealed in Table 1. Two identical 1.5 hp rated power centrifugal pumps were installed to circulate hot and cold circuits. Each loop contains bypass line and ball valve to control the flow rate directed to the shell and coil heat exchanger. Two identical variable area flow meters (Dwyer® Series Polycarbonate flow meter with stainless steel float, 1.8–18 l/min flow rate range) were used to measure the volume flow rates of the two loops.

Twenty-eight K-type thermocouples (wires of 0.1 mm diameter) were used to measure the temperatures of each heat exchanger. Four thermocouples were inserted into the flow streams, at approximately 60 mm from the heat exchanger ports, to record inlet and exit temperatures of shell and HCT fluids. Twenty thermocouples are placed on slight grooves on the external surface of HCT to measure the wall temperatures where the thermal resistance of the copper tubes can be disregarded. They were mounted at ten equally distance (441.5 mm) positions on the HCT surface, with installing two thermocouples at each position (on the outer and inner diameter of the coil). A digital thermometer with resolution of 0.1 °C was used to read all thermocouples outputs. A digital differential pressure transducer was installed for measuring the pressure drop of the pure water or $\gamma\text{-Al}_2\text{O}_3/\text{water}$ nanofluid across the HCT.

The particles used in the nanofluid experiments are gamma-alumina nan-powders ($\gamma\text{-Al}_2\text{O}_3$, supplied by Infamat® Advanced Materials Corporation, USA (99.99% purity, product code 26N-0801G, 40 nm average particle size with surface area $>200 \text{ m}^2/\text{g}$). The Thermal conductivity, density and specific heat of the nanoparticles are $36 \text{ W/m}^\circ\text{C}$, 3600 kg/m^3 and $773 \text{ J/kg}^\circ\text{C}$, respectively.

3 Experimental procedures and data reduction

After preparing the nanofluid and filling heating and cooling tanks, the heater, cooling units, and pumps were turned on. Inlet temperatures of both sides of the heat exchanger

Fig. 1 Experimental setup

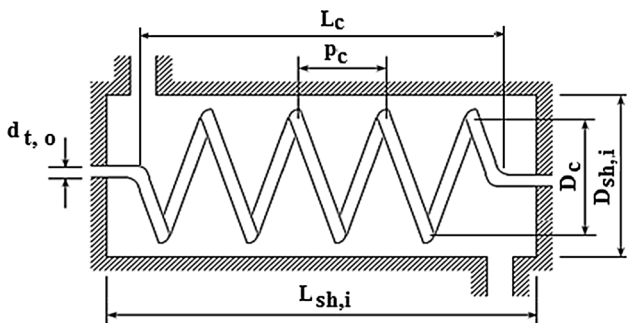
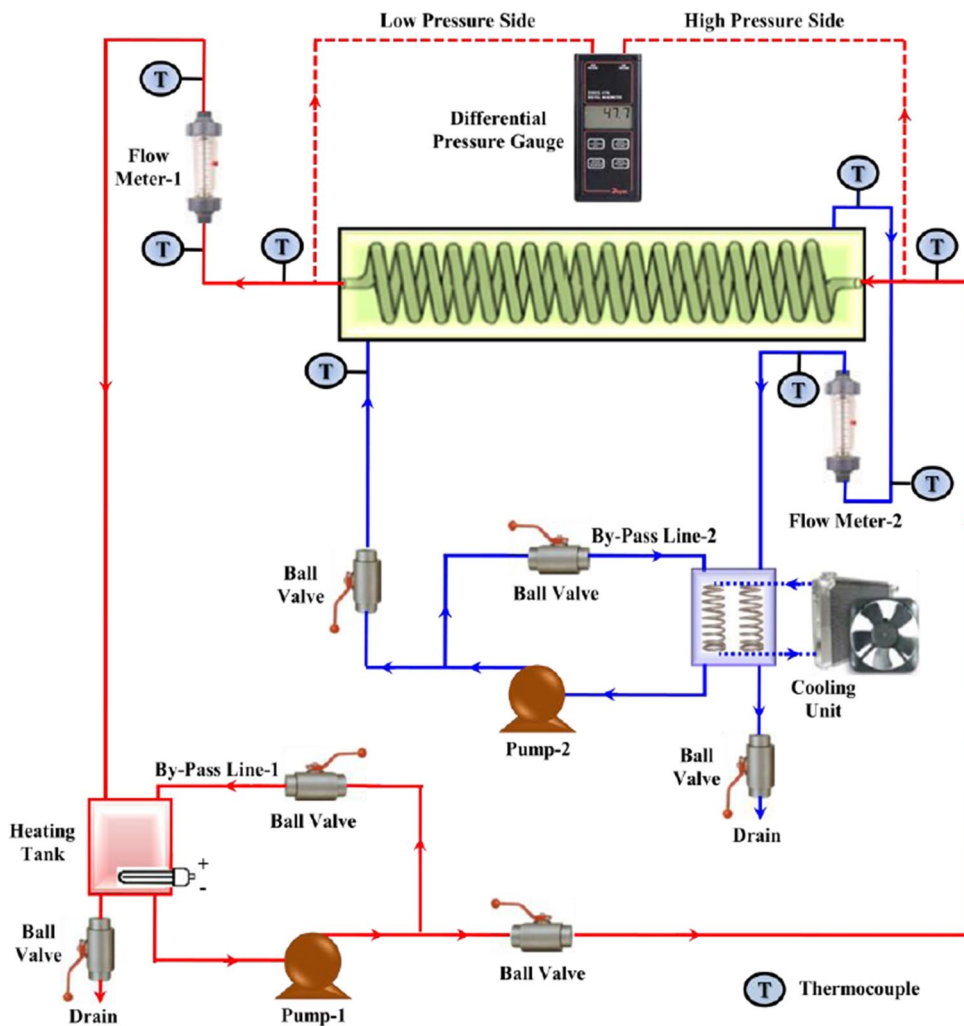


Fig. 2 Schematic diagram of the shell and coil heat exchanger

were adjusted by regulating the temperatures of the heating and cooling tanks through their thermostats. The flow rates were adjusted through flow meters and the installed valves, which were regulated to obtain the required flow rates in the primary lines. The operating conditions are given in Table 2. During the operation, the steady state condition is

conducted when the maximum variation of 0.5 °C for each thermocouple reading within 20 min.

For $\gamma\text{-Al}_2\text{O}_3/\text{water}$ nanofluid, the thermo-physical properties were calculated using the following equations [32–34].

$$k_{nf} = k_{bf} \left[\frac{k_{np} + 2k_{bf} + 2\phi(k_{np} - k_{bf})(1 - \beta)^3}{k_{np} + 2k_{bf} - \phi(k_{np} - k_{bf})(1 + \beta)^3} \right] + 5 * 10^4 \Gamma \xi \phi \rho_{bf} C_{pbf} \sqrt{\frac{\kappa T}{\rho_{np} d_{np}}} \quad (1)$$

$$\Gamma = (1722.3\phi - 134.63) - (6.04\phi - 0.4705)T \quad (2)$$

$$\xi = 0.0017(100\phi)^{-0.0841} \quad \text{for } \text{Al}_2\text{O}_3 \quad (3)$$

$$C_{pnf} = \frac{\phi(\rho_{np} C_{pnp}) + (1 - \phi)(\rho_{bf} C_{pbf})}{\rho_{nf}} \quad (4)$$

Table 1 Characteristic dimensions of the usl heat exchangers

HCT no.	D _{c,i} (mm)	D _c (mm)	δ	S (mm)	p _c (mm)	λ	L _c (mm)	L _{sh,i} (mm)	D _{sh,i} (mm)	D _{sh,h} (mm)	N
1	131.0	140.5	0.0591	10	19.52	0.0442	205	305	303	205.1	10.00
2				20	29.52	0.0669	305	405	284		
3				30	39.52	0.0895	405	505	271		
4				40	49.52	0.1122	505	605	262		
5				50	59.52	0.1348	605	705	255		

Table 2 Range of fluids operating conditions

Parameters	Range or value
HCT-side nanofluid flow rate (l/min)	1.7–11.158 (5702 ≤ Re _t ≤ 55,101)
HCT-side inlet temperature (°C)	45, 55, 65 (1.92 ≤ Pr _t ≤ 3.9)
Nanoparticles volume concentration (%)	0.5, 1, 1.5, 2
Shell-side water flow rate (l/min)	6.018
Shell-side inlet temperature (°C)	20

$$\mu_{nf} = \frac{\mu_{bf}}{[1 - \phi]^{2.5}} + 5 * 10^4 \xi \Gamma \phi \rho_{bf} \sqrt{\frac{\kappa T}{\rho_{np} d_{np}}} \quad (5)$$

$$Pr_{nf} = \frac{\mu_{nf} C_{p,nf}}{k_{nf}} \quad (6)$$

The fluid properties were calculated at the bulk temperatures, T_{sh,m} and T_{t,m}, respectively. While for pressure drop calculations, the HCT water properties were calculated at the film temperature, T_f, as recommended by Schmidt [35]. The bulk and film temperatures are calculated as follows:

$$T_{t,m} = \frac{T_{t,i} + T_{t,o}}{2} \quad (7)$$

$$T_{sh,m} = \frac{T_{sh,i} + T_{sh,o}}{2} \quad (8)$$

$$T_f = \frac{T_{t,m} + \bar{T}_{t,s}}{2} \quad (9)$$

$$\bar{T}_{t,s} = \frac{\sum T_{t,s}}{20} \quad (10)$$

The heat transfer rates on the HCT and shell sides (Q_t and Q_{sh}) were calculated by;

$$Q_t = \dot{m}_t C_{p,t} (T_{t,i} - T_{t,o}) \quad (11)$$

$$Q_{sh} = \dot{m}_{sh} C_{p,sh} (T_{sh,o} - T_{sh,i}) \quad (12)$$

$$Q_{ave} = \frac{|Q_t| + |Q_{sh}|}{2} \quad (13)$$

This heat load of the heat exchanger was used to calculate the average heat transfer coefficient for the HCT-side fluid, h_t, and then the average Nusselt number for the HCT-side fluid, Nu_t, as follows;

$$Q_{ave} = h_t A_{t,i} (T_{t,m} - \bar{T}_{t,s}) \quad (14)$$

$$Nu_t = \frac{h_t d_{t,i}}{k_t} \quad (15)$$

The overall thermal conductance was calculated from the temperature data and flow rates using Eq. (16);

$$U_o A_{t,o} = \frac{Q_{ave}}{\Delta T_{LM}} \quad (16)$$

$$\Delta T_{LM} = \frac{(\Delta T_i - \Delta T_o)}{\ln \left[\frac{\Delta T_i}{\Delta T_o} \right]} \quad (17)$$

where, ΔT_i and ΔT_o are area of the outer surface of the HCT the temperature difference at each end of the heat exchange.

HCT Reynolds number can written as follows;

$$Re_t = \frac{4\dot{m}_t}{\pi d_{t,i} \mu_t} \quad (18)$$

Fanning friction factor for the fluid in the HCT was calculated from measuring the pressure drop using the following equation;

$$f_c = \frac{\Delta P_c d_{t,i}}{2L_t \rho_t u_t^2} = \frac{\Delta P_c \pi^2 \rho_t d_{t,i}^5}{32L_t \dot{m}_t^2} \quad (19)$$

4 Uncertainty analyses

The primary parameters (Re_t, Nu_t and f_c) used to present the experimental results in this study are functions of many variables including laboratory measurement data and physical properties. Error associated with each of these measured quantities was accounted to quantify the uncertainty properly. It should be noted that according to the manufacturer, uncertainty in the HCT outer and inner diameters is ±0.01% mm, which can be neglected. The uncertainty in the measured coil and shell dimensions was assumed to be

Table 3 Average uncertainties in the main parameters

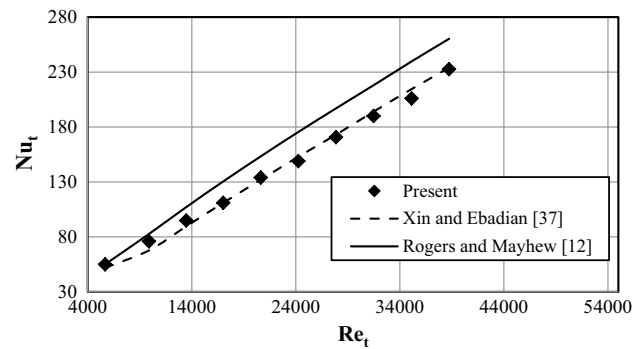
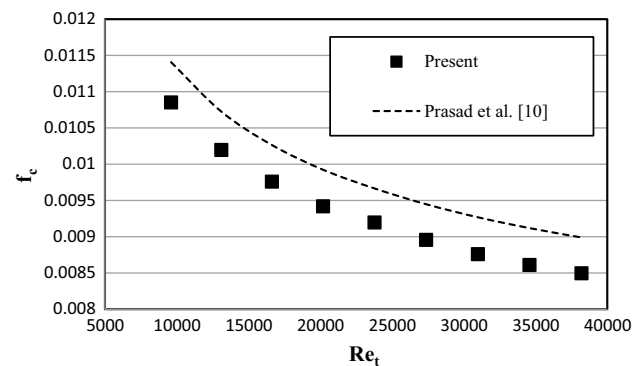
Parameter	Average uncertainty (%)	
	Water experiments	Nanofluids experiments
Reynolds numbers	± 1.7	± 1.7
HCT-side average Nusselt number	± 4.9	± 7.0
HCT-side average heat transfer coefficient	± 4.9	± 7.0
HCT-side Fanning friction factor	± 3.7	± 3.7

$\pm 0.5\%$ mm; this was guessed quantity from meter scale. The accuracy of all thermocouples is of ± 0.1 °C. In addition, the uncertainty applied to the thermal properties of pure water and nanofluid was assumed to be $\pm 0.1\%$. The nanoparticles were weighted using an electronic balance, with an accuracy of ± 0.1 g.

The uncertainties associated with estimating the volume and collecting time are ± 0.01 l and ± 1 s, respectively. With a 95% confidence level considered for normal distribution, the uncertainty is calculated based upon the root sum square combination of the effects of each of the individual measuring values presented by Kline and McClintock [36]. For all experimental runs, the uncertainties in all calculated parameters are illustrated in Table 3.

5 Results and discussion

Firstly, the obtained experimental results of Nusselt number for water were validated with the experimental data obtained by Rogers and Mayhew [12], and Xin and Ebadian [37]. In addition, another comparison of the experimental data for HCT-fanning friction factor with the results of Prasad et al. [10] was performed. As seen in Figs. 3 and 4, good agreement between the present experimental results and the previous correlations is obtained. The low values of the average uncertainties obtained in Table 3 and the good agreement previous studies reveal confidence in the experimental set up and the used measurement techniques. The present experimental setup was employed to study the effect of coil torsion and nanoparticles concentrations of $\gamma\text{-Al}_2\text{O}_3$ (40 nm)/water nanofluid that passes in HCT side with the same curvature ratio (δ) of 0.0591 within $0.0442 \leq \lambda \leq 0.1348$, $5702 \leq Re_t \leq 55,101$, $1.92 \leq Pr_t \leq 3.9$, and $0.5\% \leq \varphi \leq 2\%$. The operating conditions of the pure cold water are hold constant in the shell side at $T_{sh,i} = 20$ °C and $\dot{V}_{sh} = 6.018$ l/min as revealed in Table 2.

**Fig. 3** Validation of the experimental average Nusselt number for helically coiled tube ($T_{t,i} = 35$ °C, $T_{sh,i} = 15$ °C, $\delta = 0.0591$ and $\lambda = 0.0895$)**Fig. 4** Validation of the experimental Fanning friction factor for helically coiled tube ($T_{t,i} = 35$ °C, $T_{sh,i} = 15$ °C, $\delta = 0.0591$ and $\lambda = 0.0895$)

5.1 Effect of nanoparticles concentration

Figure 5 represents the results of h_t , Nu_t and U_o due to varying the nanoparticles concentration within $0\% \leq \varphi \leq 2\%$ at HCT inlet temperatures of 55 °C and coil specifications of $\delta = 0.0591$ and $\lambda = 0.0895$. It is illustrated that h_t , Nu_t and U_o of nanofluids are higher than that of the base fluid at same flow condition. The ratios of $h_{t,nf}/h_{t,bf}$, $Nu_{t,nf}/Nu_{t,bf}$ and $U_{o,nf}/U_{o,bf}$ reaches 3.79, 2.11 and 2.32, respectively, when φ increases from 0 to 2% at $Re_t = 42,922$. The observed enhancement of heat transfer coefficients of nanofluids can be attributed to the interactions and Brownian motion of nanoparticles and the resulting disturbance of the boundary layer in addition to the enhanced thermal conductivity of nanofluids.

Figure 6 represents the effect of nanoparticles loading on HCT-Fanning friction factor within $0 \leq \varphi \leq 2\%$ at HCT inlet temperatures of 55 °C and coil specifications (torsion

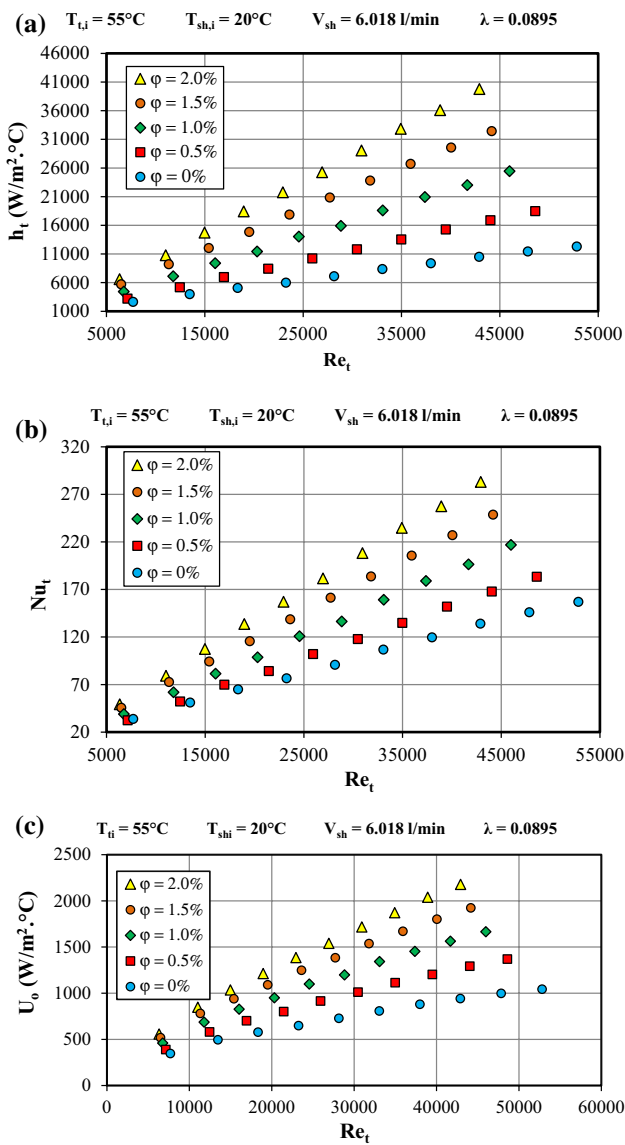


Fig. 5 Variation of HCT-average heat transfer coefficient, HCT Nusselt number and overall heat transfer coefficient with HCT-Reynolds number at different nanoparticles concentrations ($\delta = 0.0591$)

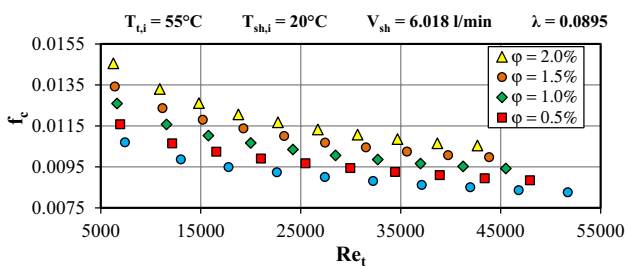


Fig. 6 Variation of HCT-Fanning friction factor with HCT-Reynolds number at different nanoparticles concentrations ($\delta = 0.0591$)

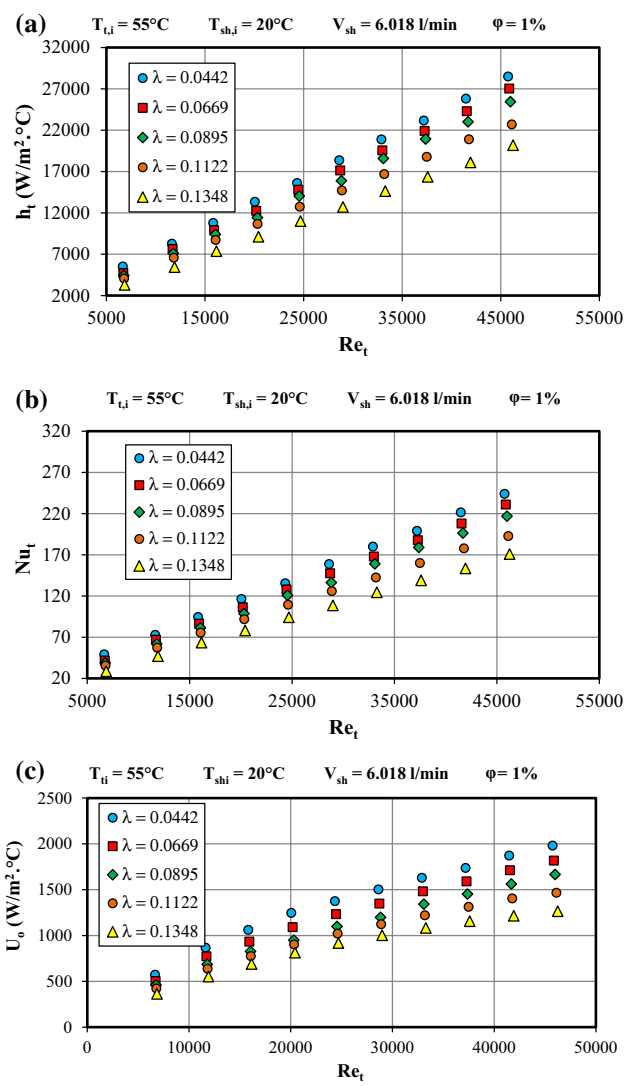


Fig. 7 Variation of HCT-average heat transfer coefficient, HCT Nusselt number and overall heat transfer coefficient with HCT-Reynolds number at different HCT-torsions ($\delta = 0.0591$)

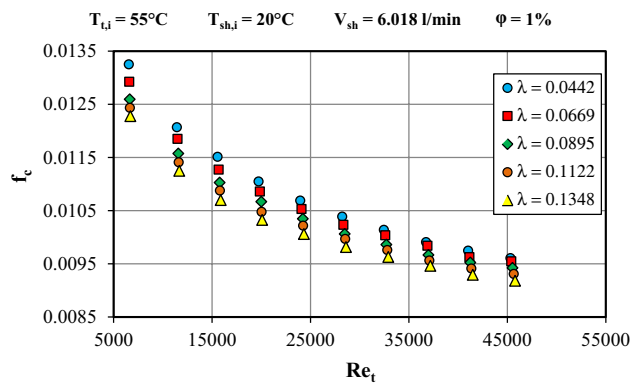


Fig. 8 Variation of HCT-Fanning friction factor with HCT-Reynolds number at different HCT-torsions ($\delta = 0.0591$)

and curvature). It is clear that f_c of nanofluids is higher than that of the base fluid at same flow condition. This can be returned to high viscosity of the nanofluid, which increases with increasing the nanoparticles loading in the base fluid. The HCT-Fanning friction factor with $\varphi = 2\%$ is 1.36 times that of base fluid ($\varphi = 0\%$) at $Re_t = 7426.3$.

5.2 Effect of coil torsion

The effects of coil torsion on the heat transfer rate and HCT Fanning friction factor are shown in Figs. 7 and 8, respectively. From Fig. 7, it is clear that increasing coil torsion decreases h_t , Nu_t and U_o at same Re_t . This can be attributed to diminishing of the centrifugal effect due to the increase in rotational force as a result of increasing the coil torsion. It is illustrated that at $Re_t = 45,750$, the ratios of $h_{t,nf}/h_{t,bf}$, $Nu_{t,nf}/Nu_{t,bf}$ and $U_{o,nf}/U_{o,bf}$ reaches 1.41, 1.43 and 1.57 when λ decreases from 0.1348 to 0.0442, respectively.

From Fig. 8, it is shown that decreasing the coil torsion leads to slight increase in f_c at the same Re_t . This can be attributed to the increase in the centrifugal force and consequently vortices formation as a result of decreasing the torsion or rotational effect. The HCT-Fanning friction factor with $\varphi = 1\%$ is 1.079 times that of base fluid ($\varphi = 0\%$) when λ decreases from 0.1348 to 0.0442 at $Re_t = 6555$.

5.3 Influence of nanofluid inlet temperature

The influence of the nanofluid inlet temperature on the thermal performance for the five heat exchanger configurations ($0.0442 \leq \lambda \leq 0.1348$) is studied for different concentrations of $\gamma\text{-Al}_2\text{O}_3$ nanoparticles $0 \leq \varphi \leq 2\%$. A sample of the obtained results of h_t , Nu_t , U_o and f_c are illustrated in Fig. 9 for $\lambda = 0.0895$ at $\delta = 0.0591$. From this figure, it is also obvious for all experiments that as the inlet temperature of the HCT-fluid flow increases, h_t , Nu_t and U_o decrease at the same Re_t . This can be attributed to the decrease in Prandtl number with increasing the temperature of the nanofluid. Also as shown in Fig. 9d, the effect of $T_{i,i}$ on f_c is nearly insignificant. This can be returned to the lower effect of viscosity variation compared with the centrifugal force.

The average increases in h_t , Nu_t , U_o and f_c at nanoparticles concentration and coil torsion limits are illustrated in Table 4.

5.4 Thermal performance index

To have an effective judgment on an enhancement heat transfer technique, the enhancement in convective heat transfer given by the nanofluid should exceed the increase in pressure drop due to the presence of Nano scale solid particles in the base fluid. The thermal performance index (TPI) is determined using h_t and the pressure drop ratios

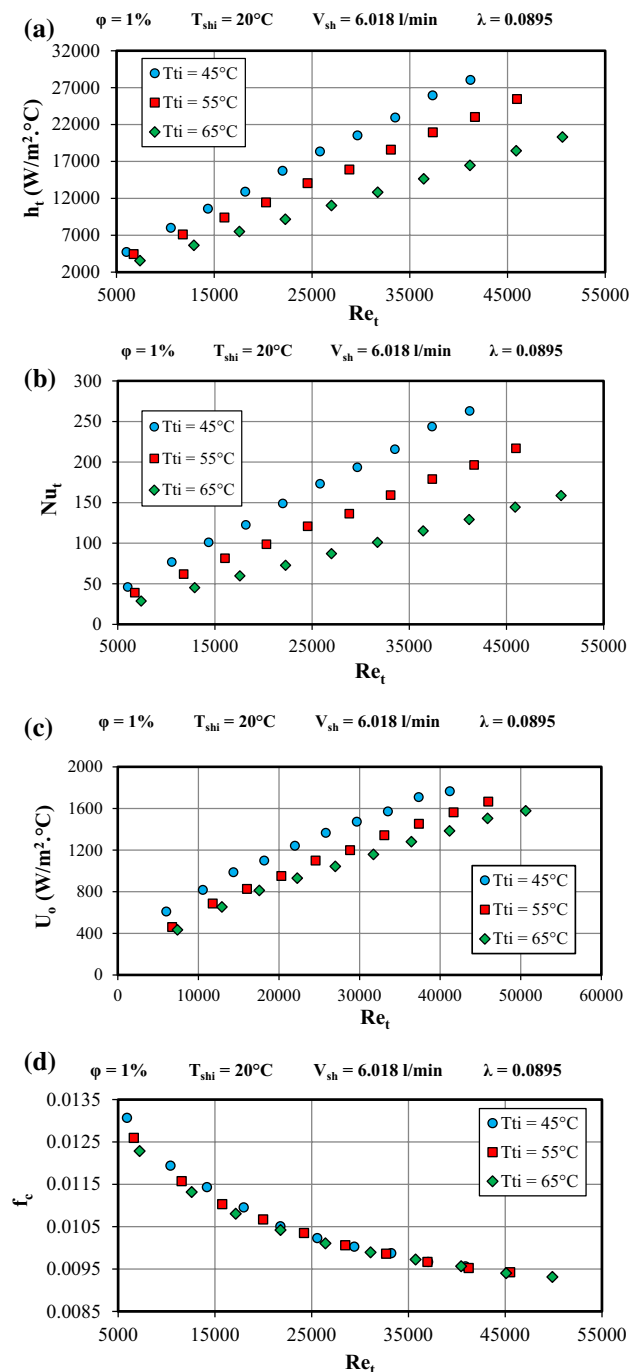


Fig. 9 Variation of HCT heat transfer coefficient, HCT Nusselt number, overall heat transfer coefficient and Fanning friction factor with HCT-Reynolds number at different HCT-inlet temperatures ($\delta = 0.0591$)

that are calculated using the values obtained for $\gamma\text{-Al}_2\text{O}_3$ (40 nm)/water nanofluid and pure water, as follows [24, 31];

$$TPI = \frac{h_{t,nf}/h_{t,bf}}{\Delta P_{c,nf}/\Delta P_{c,bf}} \quad (20)$$

Table 4 The average increases in h_t , Nu_t , U_o and f_c at the upper and lower limits of λ and φ

	$\lambda = 0.0422$		$\lambda = 0.1348$	
	$\varphi = 0.5\%$	$\varphi = 2\%$	$\varphi = 0.5\%$	$\varphi = 2\%$
h_t	28.6–36.4%	134.1–195.7%	56.9–57.1%	235.4–238.9%
Nu_t	2.6–6.5%	38–66.6%	21.7–23.5%	85.8–95.5%
U_o	15.5–23.6%	54.1–94.3%	34.7–37.9%	105.7–123.2%
f_c	7.8–10.9%	28–37.7%	5.7–8.6%	26.3–36.4%

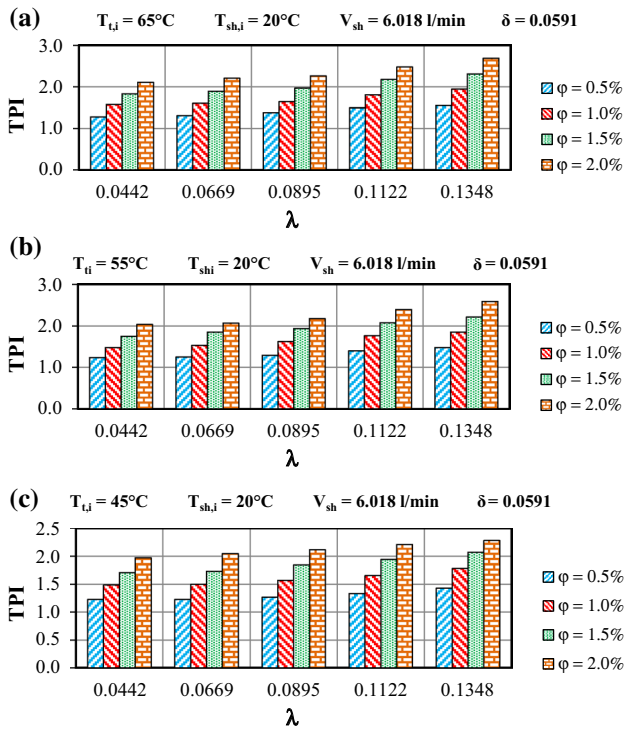


Fig. 10 Variation of the average thermal performance index with HCT-torsion at different nanoparticles concentrations ($\delta = 0.0591$). **a** $T_{t,i} = 65^\circ\text{C}$. **b** $T_{t,i} = 55^\circ\text{C}$. **c** $T_{t,i} = 45^\circ\text{C}$

Over the studied range of HCT-Reynolds number, the average TPI was calculated and the results are illustrated at different HCT-side inlet temperatures in Fig. 10 for different coil torsions and nanoparticles concentrations.

From Fig. 10, it noticed that the TPI is more than unity, which states that the enhancement in the heat transfer rate in the HCTs due to using nanofluids is higher than the corresponding increase in the pressure drop. This assures the ability of using $\gamma\text{-Al}_2\text{O}_3$ (40 nm)/water nanofluid in the HCTs with $0.5\% \leq \varphi \leq 2\%$ as a compound heat transfer enhancement technique inside shell and coil heat exchangers instead of using HCTs only. Moreover,

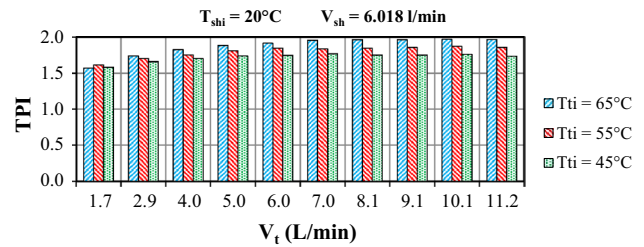


Fig. 11 Variation of the average thermal performance index with HCT-volume flow rate at different nanoparticles concentrations ($0.0442 \leq \lambda \leq 0.1348$ and $\delta = 0.0591$)

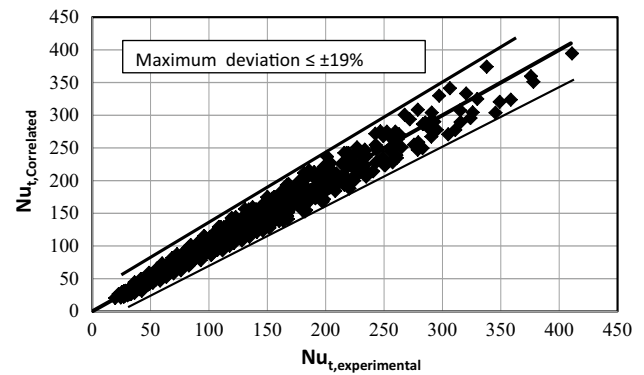


Fig. 12 Comparison of experimental values for HCT-average Nusselt number with that correlated by Eq. (21)

it is shown for all HCTs that increasing φ enhances the TPI. Over the studied range of HCT-Reynolds number, the average value of TPI is of 1.34 and 2.24 at $\varphi = 0.5\%$ and $\varphi = 2\%$, respectively, for HCTs with same δ . Additionally, for HCTs with same δ , it is clear that the TPI increases with increasing coil torsion. The average value of TPI is of 1.64 at $\lambda = 0.0442$ while its average value at $\lambda = 0.1348$ is of 2.01.

Furthermore, over the studied range of HCT-geometrical parameters and nanoparticles concentrations, the average TPI was calculated and illustrated for different HCT-side flow rates in Fig. 11. It evident that increasing the HCT-side flow rate slightly enhances the thermal performance index at lower flow rate, and this enhancement goes up as HCT-side flow rate increases. For HCTs with same δ , the average value of TPI is of 1.59 and 1.85 at \dot{V}_t of 1.7 and 11.16 l/min, respectively.

Moreover, it is observed in Figs. 10 and 11 that increasing HCT-side inlet temperature slightly enhances the thermal performance index. For HCTs with same δ , the average value of TPI is of 1.72–1.87 when $T_{t,i}$ varies from 45 to 65 $^\circ\text{C}$, respectively.

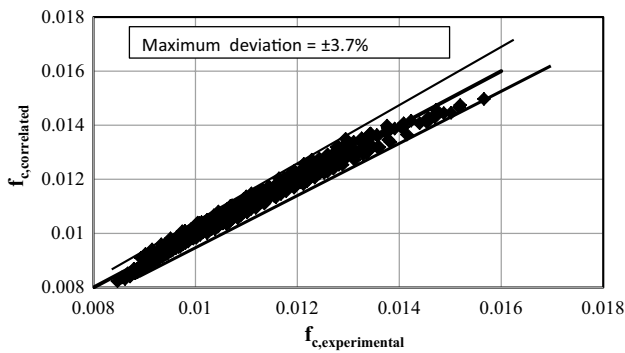


Fig. 13 Comparison of experimental values for HCT-fanning friction factor with that correlated by Eq. (22)

5.5 Correlations for average Nusselt numbers and friction factor

The HCT average Nusselt number is correlated as a function of HCT Reynolds and Prandtl numbers, coil torsion and nanoparticles volume concentration as follows;

$$Nu_t = 0.01974 Re_t^{0.928} Pr_t^{1.302} \lambda^{-0.2838} \varphi^{0.603} \quad (21)$$

Equation (21) is applicable for $5702 \leq Re_t \leq 55,101$, $1.92 \leq Pr_t \leq 3.9$, $0.0442 \leq \lambda \leq 0.1348$ and $0.005 \leq \varphi \leq 0.02$. Moreover, a correlation for Fanning friction factor in the HCT was obtained within $5646 \leq Re_t \leq 54,108$, $0.0442 \leq \lambda \leq 0.1348$ and $0.005 \leq \varphi \leq 0.02$, as follows;

$$f_c = 0.087 Re_t^{-0.1644} \lambda^{-0.04775} \varphi^{0.1246} \quad (22)$$

Comparisons of the present experimental HCT-average Nusselt number and Fanning-friction factor with those calculated by the proposed correlations are shown in Figs. 12 and 13.

From Figs. 12 and 13, it is evident that the proposed correlations are in good agreement with the present experimental data. It is clearly seen that the data of the proposed equations falls within maximum deviation of ± 19 and $\pm 3.7\%$ for Nu_t and f_c , respectively.

6 Conclusions

The present work was carried out to investigate the convective heat transfer characteristics in shell and coil heat exchanger inside the HCTs. The investigated operating parameters were $5702 \leq Re_t \leq 55,101$, $1.92 \leq Pr_t \leq 3.9$, $0.0442 \leq \lambda \leq 0.1348$ and $0.5\% \leq \varphi \leq 2\%$. The main conclusions from this investigation are:

1. For all HCT-geometric variables and operating conditions, utilization of $\gamma\text{-Al}_2\text{O}_3$ (40 nm)/water nanofluid

with $0.5\% \leq \varphi \leq 2\%$ instead of pure water in the HCTs results in remarkable heat transfer enhancement; this goes up as the nanoparticle concentration increases.

2. For same operating conditions, reducing the coil torsion enhances the heat transfer rate of nanofluids and increases the HCT-friction factor for base fluids as well as nanofluids.
3. For all HCT-geometric variables, the heat transfer rate goes up as the mass flow rate increases and as the fluid inlet temperature decreases. The effect of HCT-fluid inlet temperature on the HCT-friction factor is nearly insignificant especially at higher Re_t .
4. For all geometric variables and operating conditions, utilization of $\gamma\text{-Al}_2\text{O}_3$ (40 nm)/water nanofluid with $0.5\% \leq \varphi \leq 2\%$ instead of pure water in the HCTs results in remarkable HCT-friction factor increase.
5. For all coil torsions, nanoparticle concentrations and operating conditions, the thermal performance index is more than unity. Therefore, this assures the ability of using $\gamma\text{-Al}_2\text{O}_3$ (40 nm)/water nanofluid in the HCTs with $0.5\% \leq \varphi \leq 2\%$ as a compound heat transfer enhancement technique inside shell and coil heat exchangers instead of using HCTs only.
6. The thermal performance index increases with increasing nanoparticles concentration, coil torsion and HCT-side inlet temperature and flow rate.
7. Correlations for the HCT-average Nusselt number and fanning friction factor as a function of the investigated parameters are obtained.

References

1. Bai B, Guo L, Feng Z, Chen X (1999) Turbulent heat transfer in a horizontally coiled tube. *Heat Transfer Asian Res* 28(5):395–403
2. Sandeep KP, Palazoglu TK (1999) Secondary flow in coiled tubes, ASAE, 2950 Niles Rd., St. Joseph, MI 49085–9659 USA
3. Genssle A, Stephan K (2000) Analysis of the process characteristics of an absorption heat transformer with compact heat exchangers and the mixture TFE-E181. *Int J Therm Sci* 39(1):30–38
4. Kern DQ (2000) Process heat transfer, 4th reprint edn. Tata McGraw-Hill, New York
5. Rennie TJ (2004) Numerical and experimental studies of a double-pipe helical heat exchanger. Department of Bioresource Engineering, McGill University, Montreal
6. Kumar V, Saini S, Sharma M, Nigam KDP (2006) Pressure drop and heat transfer study in tube-in-tube helical heat exchanger. *Chem Eng Sci* 61(13):4403–4416
7. Chingulpitak V, Wongwises S (2010) Effects of coil diameter and pitch on the flow characteristics of alternative refrigerants flowing through adiabatic helical capillary tubes. *Int Commun Heat Mass Transf* 37(9):1305–1311
8. Chingulpitak S, Wongwises S (2011) A comparison of flow characteristics of refrigerants flowing through adiabatic straight and helical capillary tubes. *Int Commun Heat Mass Transf* 38(3):398–404

9. Huminic G, Huminic A (2011) Heat transfer characteristics in double tube helical heat exchangers using nanofluids. *Int J Heat Mass Transf* 54(20):4280–4287
10. Prasad BV, Das DH, Prabhakar AK (1989) Pressure drop, heat transfer and performance of a helically coiled tubular exchanger. *Heat Recovery Syst CHP* 9(3):249–256
11. Zhao Z, Wang X, Che D, Cao Z (2011) Numerical studies on flow and heat transfer in membrane helical-coil heat exchanger and membrane serpentine-tube heat exchanger. *Int Commun Heat Mass Transf* 38(9):1189–1194
12. Rogers GF, Mayhew YR (1964) Heat transfer and pressure loss in helically coiled tubes with turbulent flow. *Int J Heat Mass Transf* 7(11):1207–1216
13. Li Q, Xuan Y (2002) Convective heat transfer and flow characteristics of Cu–water nanofluid. *Sci China Ser E Technol Sci* 45(4):408–416
14. Manca O, Jaluria Y, Poulikakos D (2010) Heat transfer in nanofluids, *Adv Mech Eng* 2010. Article ID 380826
15. Das SK, Choi SU, Yu W, Pradeep T (2007) *Nanofluids: science and technology*. Wiley, Hoboken
16. Zamzamin A, Oskouie SN, Doosthoseini A, Joneidi A, Pazouki M (2011) Experimental investigation of forced convective heat transfer coefficient in nanofluids of Al_2O_3/EG and CuO/EG in a double pipe and plate heat exchangers under turbulent flow. *Exp Therm Fluid Sci* 35:495–502
17. Peyghambarzadeh SM, Hashemabadi SH, Hoseini SM, Seifi Jamnani M (2010) Experimental study of heat transfer enhancement using water/ethylene glycol based nanofluids as a new coolant for car radiators. *Int Commun Heat Mass Transf* 38:1283–1290
18. Peyghambarzadeh SM, Jamnani MS (2011) Improving the cooling performance of automobile radiator with Al_2O_3 /water nanofluid. *Appl Therm Eng* 31:1833–1838
19. Razi P, Akhavan-Behabadi MA, Saeednia M (2011) Pressure drop and thermal characteristics of CuO–base oil nanofluid laminar flow in flattened tubes under constant heat flux. *Int Commun Heat Mass Transf* 38:964–971
20. Moraveji MK, Haddad SMH, Darab M (2012) Modeling of forced convective heat transfer of a non-Newtonian nanofluid in the horizontal tube under constant heat flux with computational fluid dynamics. *Int Commun Heat Mass Transf* 39:995–999
21. Hussein AM, Bakar RA, Kadirgama K (2014) Study of forced convection nanofluid heat transfer in the automotive cooling system. *Case Stud Therm Eng* 2:50–61
22. Kumar KP, Saibabu J, Rao KV, Srikanth DN (2008) Experimental analysis of sisal nanofluids in shell and coil heat exchanger. *Int J Nanosyst* 1(1):87–90
23. Huminic G, Huminic A (2011) A heat transfer characteristics in double tube helical heat exchangers using nanofluids. *Int J Heat Mass Transf* 54(19–20):4280–4287
24. Hashemi SM, Akhavan-Behabadi MA (2012) An empirical study on heat transfer and pressure drop characteristics of CuO–base oil nanofluid Flow in a horizontal helically coiled tube under constant heat flux. *Int Commun Heat Mass Transf* 39:144–151
25. Kumar PCM, Kumar J, Suresh S (2012) Heat transfer and friction factor studies in helically coiled tube using Al_2O_3 /water nanofluid. *Eur J Sci Res* 82(2):161–172
26. Kumar PCM, Kumar J, Suresh S, Babu KP (2012) Experimental study on parallel and counter flow configuration of a shell and helically coiled tube heat exchanger using Al_2O_3 /water nanofluid. *J Mater Environ Sci* 3(4):766–775
27. Kumar PCM, Kumar J, Suresh S, Babu KP (2012) Heat transfer enhancement in a helically coiled tube with Al_2O_3 /water nanofluid under laminar flow condition. *Eur J Sci Res* 82(2):161–172
28. Kumar PCM, Kumar J, Suresh S (2013) Experimental investigation on convective heat transfer and friction factor in a helically coiled tube with Al_2O_3 /water nanofluid. *J Mech Sci Technol* 27(1):239–245
29. Salem MR, Elshazly KM, Sakr RY, Ali RK (2016) Effect of oil torsion on heat transfer and pressure drop characteristics of shell and coil heat exchanger. *J Therm Sci Eng Appl Trans ASME* 8(1–7):011015
30. Salem MR, Elshazly KM, Sakr RY, Ali RK (2015) Experimental investigation of coil curvature effect on heat transfer and pressure drop characteristics of shell and coil heat exchanger. *J Therm Sci Eng Appl Trans ASME* 7(1–9):011005
31. Salem MR, Elshazly KM, Sakr RY, Ali RK (2015) Effect of $\gamma-Al_2O_3$ /water nanofluid on heat transfer and pressure drop characteristics of shell and coil heat exchanger with different coil curvatures. *J Therm Sci Eng Appl Trans ASME* 7(1–9):041009
32. Koo J, Kleinstreuer C (2004) A new thermal conductivity model for nanofluids. *J Nanopart Res* 6(6):577–588
33. Koo J, Kleinstreuer C (2005) Laminar nanofluid flow in micro-heat-sinks. *Int J Heat Mass Transf* 48(13):2652–2661
34. Xuan Y, Roetzel W (2000) Conceptions for heat transfer correlation of nanofluids. *Int J Heat Mass Transf* 43(19):3701–3707
35. Schmidt E (1967) Heat transfer and pressure loss in spiral tubes. *Chem Eng Technol* 39:781–789
36. Kline SJ, McClintock FA (1953) Describing uncertainties in single-sample experiments. *Mech Eng* 75(1):3–8
37. Xin RC, Ebadian MA (1997) The effects of Prandtl numbers on local and average convective heat transfer characteristics in helical pipes. *J Heat Transf (ASME)* 119(3):467–473